

NUMERICAL SOLUTION OF POLYMER SELF-CONSISTENT FIELD THEORY*

HECTOR D. CENICEROS[†] AND GLENN H. FREDRICKSON[‡]

Abstract. We propose efficient pseudospectral numerical schemes for solving the self-consistent, mean-field equations for inhomogeneous polymers. In particular, we introduce a robust class of semi-implicit methods that employ asymptotic small scale information about the nonlocal density operators. The relaxation schemes are further embedded in a multilevel strategy resulting in a method that can cut down the computational cost by an order of magnitude. Three illustrative problems are used to test the numerical methods: (i) the problem of finding the mean chemical potential field for a prescribed inhomogeneous density of homopolymers; (ii) an incompressible melt blend of two chemically distinct homopolymers; and (iii) an incompressible melt of AB diblock copolymers.

Key words. diblock copolymers, incompressible melt blend, semi-implicit methods, multilevel relaxation

AMS subject classifications. 65K10, 65Z05

DOI. 10.1137/030601338

1. Introduction. Field-theoretic models and approaches have proven to be very useful in the study of inhomogeneous polymer and complex fluid phases. The application of such methods to dense phases, such as melts and concentrated solutions of homo-, block-, and graft copolymers, has been particularly fruitful in unraveling the complexities of equilibrium self-assembly in such systems [15, 18, 16, 21, 9, 19]. Normally the statistical field theory models are solved in the mean-field (saddle point) approximation, although recent developments enable direct numerical simulation of field theories without any simplifying approximations [13, 11, 7]. Here we shall be concerned with the development of efficient numerical algorithms for solving equilibrium field theories in the mean-field approximation, the so-called self-consistent field theory (SCFT), that is well known in the fields of polymer and colloid science.

The SCFT equations are a highly nonlinear set of equations in one or more chemical potential fields. The equations have also a strong nonlocality that emerges from the solution of a modified diffusion equation and reflects the connected nature of a polymer over distances of order, its radius-of-gyration. Solutions for the potential fields, in turn, uniquely specify the equilibrium monomer densities of the different species and other thermodynamic and structural quantities of interest. Two strategies for solving the SCFT equations have emerged: a *spectral* approach heavily exploited by Matsen and Schick [20, 21] and a *real-space* approach followed by Scheutjens and Fleer [25], Fraaije [8], Fraaije et al. [9], Shi, Noolandi, and Desai [26], Whitmore and Vavasour [29], and Drolet and Fredrickson [5, 6], among others. A disadvantage of the fully spectral approach is that the computational effort scales poorly [as $O(N_x^3)$] with the number of spectral elements N_x . It is therefore not well suited to high-resolution simulations where there is no advanced knowledge of the symmetries of

*Received by the editors October 22, 2003; accepted for publication (in revised form) February 23, 2004; published electronically June 15, 2004. This work was partially supported by the National Science Foundation under award CTS-0304596 for Nanoscale Exploratory Research.

<http://www.siam.org/journals/mms/2-3/60133.html>

[†]Department of Mathematics, University of California, Santa Barbara, CA 93106-5080 (hdc@math.ucsb.edu).

[‡]Departments of Chemical Engineering & Materials and Materials Research Laboratory, University of California, Santa Barbara, CA 93106-5080 (ghf@mc-cam.ucsb.edu).

candidate structures. The real space method is better suited for situations where the symmetries are not known in advance but becomes computationally demanding in three dimensions. Recent work by Rasmussen and Kalosakas [24] has shown that the solution of the modified diffusion equation can be efficiently solved by a *pseudospectral* technique, taking advantage of the best features of real and reciprocal space. Here we argue that this philosophy can be fruitfully extended to the full solution of the SCFT equations, including both the solution of the diffusion equation as well as optimization of the chemical potential fields.

2. Models of inhomogeneous polymers. In the present paper we consider three illustrative problems that are typical of those encountered in applying SCFT to realistic polymer systems. These problems are the following:

1. *Target homopolymer density problem.* Find the equilibrium chemical potential field $\mu(\mathbf{r})$ that produces a prescribed monomer density profile $\rho(\mathbf{r})$.
2. *Incompressible A+B homopolymer blend.* Find the chemical potential fields $\mu_A(\mathbf{r})$ and $\mu_B(\mathbf{r})$ that produce the lowest free energy spatial distribution of type A and B segments in a blend of homopolymers, subject to a local constraint of incompressibility.
3. *Incompressible AB diblock copolymer melt.* Find the chemical potential fields $\mu_A(\mathbf{r})$ and $\mu_B(\mathbf{r})$ that produce the lowest free energy spatial distribution of type A and B segments of a diblock copolymer, subject to a local constraint of incompressibility.

The first problem is the simplest of the three since a unique chemical potential field exists for a given target density pattern. However, it is a particularly important problem in extending SCFT to dynamics [8, 9, 10], since the density field is more natural for building models of kinetic evolution, yet the chemical potential field is required at each time step to embed accurate thermodynamic forces. Problems 2 and 3 require a simultaneous adjustment of the chemical potential fields and the conjugate densities in order to reach a local minimum of the free energy functional. Ideally in such problems one would like a global, rather than local, minimum of the free energy, but this is an issue beyond the scope of the present paper and that often must be sorted out with physical intuition. In problem 2, the equilibrium density pattern reflects a *macroscopic phase separation* [3] between the two components and a long-wavelength instability of the energy functional. In contrast, problem 3 involves a finite-wavelength instability associated with *microphase separation* [18] of the block copolymer melt. In problems 2 and 3, as we shall discuss, the optimization is complicated by the saddle point character of the physically relevant solutions.

We now turn to the specific models under investigation. We follow closely the notation in a recent review [11] and in all cases work in the canonical ensemble.

2.1. Target homopolymer density model. We consider a collection of n flexible homopolymers, each of degree of polymerization N , in a volume V . Of interest is the functional (not strictly a free energy for this simple model):

$$(2.1) \quad G[\mu] = \int d\mathbf{r} \mu(\mathbf{r})\rho(\mathbf{r}) + nN \ln Q[\mu],$$

where $\rho(\mathbf{r})$ is a *prescribed* monomer density field and $Q[\mu]$ is the partition function of a single polymer subject to a chemical potential field $\mu(\mathbf{r})$. In the continuous Gaussian chain model of flexible polymers [4], $Q[\mu]$ is given by

$$(2.2) \quad Q[\mu] = \frac{1}{V} \int d\mathbf{r} q(\mathbf{r}, 1; [\mu]),$$

where the chain propagator $q(\mathbf{r}, s; [\mu])$ satisfies

$$(2.3) \quad \frac{\partial}{\partial s} q(\mathbf{r}, s; [\mu]) = \nabla^2 q(\mathbf{r}, s; [\mu]) - \mu(\mathbf{r}) q(\mathbf{r}, s; [\mu]), \quad q(\mathbf{r}, 0; [\mu]) = 1.$$

Here we have expressed the chain contour variable s in units of N and have expressed all lengths in units of the unperturbed radius-of-gyration of a polymer, $R_g = (Nb^2/6)^{1/2}$, where b is the statistical segment length.

The functional $G[\mu]$ has a *minimum*, corresponding to the potential field $\mu^*(\mathbf{r})$ satisfying

$$(2.4) \quad \left. \frac{\delta G[\mu]}{\delta \mu(\mathbf{r})} \right|_{\mu=\mu^*} = \rho(\mathbf{r}) - \tilde{\rho}(\mathbf{r}; [\mu^*]) = 0,$$

where $\tilde{\rho}(\mathbf{r}; [\mu])$ is a *monomer density operator*, reflecting the monomer density generated by a potential field $\mu(\mathbf{r})$. This operator is defined by

$$(2.5) \quad \tilde{\rho}(\mathbf{r}; [\mu]) = -nN \frac{\delta \ln Q[\mu]}{\delta \mu(\mathbf{r})} = \frac{\rho_0}{Q[\mu]} \int_0^1 ds q(\mathbf{r}, s; [\mu]) q(\mathbf{r}, 1-s; [\mu]),$$

where $\rho_0 \equiv nN/V = V^{-1} \int d\mathbf{r} \rho(\mathbf{r})$ is the volume-averaged monomer density in the system.

While $G[\mu]$ is convex, the extremum chemical potential $\mu^*(\mathbf{r})$ is not unique because $G[\mu]$ and $\tilde{\rho}(\mathbf{r}; [\mu])$ are invariant to *uniform* chemical potential shifts, $\mu(\mathbf{r}) \rightarrow \mu(\mathbf{r}) + \mu_0$. We arbitrarily choose to lift this degeneracy by requiring that $\mu^*(\mathbf{r})$ have vanishing spatial average, $V^{-1} \int d\mathbf{r} \mu^*(\mathbf{r}) = 0$.

2.2. Binary homopolymer blend model. This model corresponds to a blend of type A and B homopolymers subject to a local incompressibility constraint. For simplicity, we restrict our attention to the case of symmetric chain lengths $N_A = N_B \equiv N$ and statistical segment lengths $b_A = b_B \equiv b$. A (composition independent) Flory χ parameter is used to describe the strength of binary contacts between A and B segments [3]. In the mean-field approximation, the free energy for such a system can be expressed by the following functional:

$$(2.6) \quad F[\mu_A, \mu_B] = \int d\mathbf{r} [-f\mu_A - (1-f)\mu_B + (\mu_A - \mu_B)^2/(4\chi N)] - fV \ln Q[\mu_A] - (1-f)V \ln Q[\mu_B],$$

where V is the system volume, f is the average volume fraction of type A chains, and $Q[\mu]$ is the single chain partition function defined by (2.2) and (2.3). For the case of equal amounts of the A and B homopolymers, $f = 1/2$, this model exhibits a macroscopic phase separation into coexisting A-rich and B-rich phases for “segregation strengths” χN exceeding 2. Because of the particular orientation of the mean potential fields in the complex plane [11], physical solutions correspond to *saddle points* in which $F[\mu_A, \mu_B]$ is *minimized* with respect to the “exchange” potential field $\mu_-(\mathbf{r}) \equiv [\mu_B(\mathbf{r}) - \mu_A(\mathbf{r})]/2$ and *maximized* with respect to the “pressure” field $\mu_+(\mathbf{r}) \equiv [\mu_A(\mathbf{r}) + \mu_B(\mathbf{r})]/2$. It is the latter field that imposes the incompressibility constraint and produces the saddle point character of the problem. Relevant functional derivatives are

$$(2.7) \quad \frac{\delta F[\mu_+, \mu_-]}{\delta \mu_+(\mathbf{r})} = \tilde{\phi}_A(\mathbf{r}; [\mu_+ - \mu_-]) + \tilde{\phi}_B(\mathbf{r}; [\mu_+ + \mu_-]) - 1,$$

$$(2.8) \quad \frac{\delta F[\mu_+, \mu_-]}{\delta \mu_-(\mathbf{r})} = (2f - 1) + \frac{2}{\chi N} \mu_-(\mathbf{r}) + \tilde{\phi}_B(\mathbf{r}; [\mu_+ + \mu_-]) - \tilde{\phi}_A(\mathbf{r}; [\mu_+ - \mu_-]),$$

where $\tilde{\phi}_A$ and $\tilde{\phi}_B$ are operators giving the *local monomer volume fractions* as functionals of the potential fields. These are given by formulas similar to (2.5):

$$(2.9) \quad \tilde{\phi}_A(\mathbf{r}; [\mu_A]) = \frac{f}{Q[\mu_A]} \int_0^1 ds \, q(\mathbf{r}, s; [\mu_A]) q(\mathbf{r}, 1-s; [\mu_A]),$$

$$(2.10) \quad \tilde{\phi}_B(\mathbf{r}; [\mu_B]) = \frac{(1-f)}{Q[\mu_B]} \int_0^1 ds \, q(\mathbf{r}, s; [\mu_B]) q(\mathbf{r}, 1-s; [\mu_B]).$$

The SCFT equations to be solved for the saddle point fields $\mu_+^*(\mathbf{r})$ and $\mu_-^*(\mathbf{r})$ are obtained by setting the right-hand sides (RHSs) of (2.7) and (2.8) to zero:

$$(2.11) \quad \tilde{\phi}_A(\mathbf{r}; [\mu_+^* - \mu_-^*]) + \tilde{\phi}_B(\mathbf{r}; [\mu_+^* + \mu_-^*]) - 1 = 0,$$

$$(2.12) \quad (2f-1) + \frac{2}{\chi N} \mu_-^*(\mathbf{r}) + \tilde{\phi}_B(\mathbf{r}; [\mu_+^* + \mu_-^*]) - \tilde{\phi}_A(\mathbf{r}; [\mu_+^* - \mu_-^*]) = 0.$$

2.3. Diblock copolymer melt model. This model corresponds to a melt of flexible AB diblock copolymers subject to a local incompressibility constraint. For simplicity, we again restrict our attention to the case of symmetric statistical segment lengths $b_A = b_B \equiv b$ and employ a (composition independent) Flory χ parameter to describe the strength of binary contacts between A and B segments. The relevant free energy can be expressed by the following functional:

$$(2.13) \quad H[\mu_A, \mu_B] = \int d\mathbf{r} \, [-f\mu_A - (1-f)\mu_B + (\mu_A - \mu_B)^2/(4\chi N)] - V \ln Q_c[\mu_A, \mu_B],$$

where V is the system volume, N is the copolymer degree of polymerization, f is the average volume fraction of type A blocks, and $Q_c[\mu_A, \mu_B]$ is the partition function for a single copolymer experiencing chemical potentials μ_A and μ_B that exert forces, respectively, on the A and B blocks. This object is given by

$$(2.14) \quad Q_c[\mu_A, \mu_B] = \frac{1}{V} \int d\mathbf{r} \, q(\mathbf{r}, 1; [\mu_A, \mu_B]),$$

where the copolymer propagator satisfies

$$(2.15) \quad \frac{\partial}{\partial s} q(\mathbf{r}, s) = \nabla^2 q(\mathbf{r}, s) - \psi(\mathbf{r}, s) q(\mathbf{r}, s), \quad q(\mathbf{r}, 0) = 1,$$

and we have suppressed the functional dependence on the potentials. The function $\psi(\mathbf{r}, s)$ is given by

$$(2.16) \quad \psi(\mathbf{r}, s) \equiv \begin{cases} \mu_A(\mathbf{r}), & 0 \leq s \leq f, \\ \mu_B(\mathbf{r}), & f < s \leq 1. \end{cases}$$

For the case of a symmetric diblock copolymer melt, $f = 1/2$, this model exhibits a microphase phase separation [18] into a lamellar phase for segregation strengths χN exceeding 10.495. As in the case of the binary blend, the copolymer problem has a saddle point character in which $H[\mu_A, \mu_B]$ is to be minimized with respect to the exchange potential $\mu_-(\mathbf{r}) \equiv [\mu_B(\mathbf{r}) - \mu_A(\mathbf{r})]/2$ and maximized with respect to the

pressure $\mu_+(\mathbf{r}) \equiv [\mu_A(\mathbf{r}) + \mu_B(\mathbf{r})]/2$. The first derivatives for the diblock copolymer melt are

$$(2.17) \quad \frac{\delta H[\mu_+, \mu_-]}{\delta \mu_+(\mathbf{r})} = \bar{\phi}_A(\mathbf{r}; [\mu_\pm]) + \bar{\phi}_B(\mathbf{r}; [\mu_\pm]) - 1,$$

$$(2.18) \quad \frac{\delta H[\mu_+, \mu_-]}{\delta \mu_-(\mathbf{r})} = (2f - 1) + \frac{2}{\chi N} \mu_-(\mathbf{r}) + \bar{\phi}_B(\mathbf{r}; [\mu_\pm]) - \bar{\phi}_A(\mathbf{r}; [\mu_\pm]).$$

The local volume fraction operators $\bar{\phi}_A$ and $\bar{\phi}_B$ are given by formulas similar to (2.9) and (2.10):

$$(2.19) \quad \bar{\phi}_A(\mathbf{r}; [\mu_\pm]) = \frac{1}{Q_c[\mu_\pm]} \int_0^f ds \, q(\mathbf{r}, s; [\mu_\pm]) q^\dagger(\mathbf{r}, 1 - s; [\mu_\pm]),$$

$$(2.20) \quad \bar{\phi}_B(\mathbf{r}; [\mu_\pm]) = \frac{1}{Q_c[\mu_\pm]} \int_f^1 ds \, q(\mathbf{r}, s; [\mu_\pm]) q^\dagger(\mathbf{r}, 1 - s; [\mu_\pm]).$$

Because of the lack of head-to-tail symmetry of a diblock copolymer, a new propagator q^\dagger appears in these equations. It satisfies the modified diffusion equation

$$(2.21) \quad \frac{\partial}{\partial s} q^\dagger(\mathbf{r}, s) = \nabla^2 q^\dagger(\mathbf{r}, s) - \psi^\dagger(\mathbf{r}, s) q^\dagger(\mathbf{r}, s), \quad q^\dagger(\mathbf{r}, 0) = 1,$$

with

$$(2.22) \quad \psi^\dagger(\mathbf{r}, s) \equiv \begin{cases} \mu_B(\mathbf{r}), & 0 \leq s \leq 1 - f, \\ \mu_A(\mathbf{r}), & 1 - f < s \leq 1. \end{cases}$$

The SCFT equations for the saddle point fields are obtained as before by setting the RHSs of (2.17) and (2.18) to zero:

$$(2.23) \quad \bar{\phi}_A(\mathbf{r}; [\mu_\pm^*]) + \bar{\phi}_B(\mathbf{r}; [\mu_\pm^*]) - 1 = 0,$$

$$(2.24) \quad (2f - 1) + \frac{2}{\chi N} \mu_-^*(\mathbf{r}) + \bar{\phi}_B(\mathbf{r}; [\mu_\pm^*]) - \bar{\phi}_A(\mathbf{r}; [\mu_\pm^*]) = 0.$$

We note that one way to assess the character (convexity) of functionals such as F and H is by linearization about stationary points (see, e.g., [11]). However, to our knowledge, there is no general study to address this question.

3. Numerical methods. Efficient evaluation of the energy functionals and first derivatives of the three models requires an effective strategy for solving the modified diffusion equations (2.3), (2.15), and (2.21). Spectral methods, which typically exhibit exponential convergence in the number of retained modes, N_x , are clearly desirable for high spatial resolution two- and three-dimensional calculations in simple geometries. However, the linear operators ∇^2 and $\mu(\mathbf{r})$ (or ψ or ψ^\dagger) appearing in the diffusion equations are not simultaneously diagonal in either real or reciprocal space. As discussed recently by Rasmussen and Kalosakas [24], a pseudospectral [14] splitting scheme can be devised that preserves spectral accuracy in space and has high-order accuracy in the contour variable s . Moreover, this scheme is conveniently and efficiently implemented with fast Fourier transforms (FFTs). Specifically, (2.3) is solved by stepping forward in s from the initial condition by means of the formula

$$(3.1) \quad q(\mathbf{r}, s + \Delta s) \approx \exp[-\Delta s \mu(\mathbf{r})/2] \exp[\Delta s \nabla^2] \exp[-\Delta s \mu(\mathbf{r})/2] q(\mathbf{r}, s),$$

with errors that are third order in the contour step Δs . The first and third propagators on the RHS, $\exp[-\Delta s \mu(\mathbf{r})/2]$, are applied at collocation points in real space where they are diagonal, and the second propagator, $\exp[\Delta s \nabla^2]$, is applied in k -space by means of an FFT. For cases of periodic boundary conditions, plane wave bases are employed; for nonperiodic boundary conditions, Chebyshev polynomials collocated on the nodes of cosines prove most convenient [14]. This algorithm is unconditionally stable in any number of dimensions and is considerably more accurate than finite difference schemes based on forward time centered space, Crank–Nicolson, or Dufort–Frankel contour stepping. Furthermore, the pseudospectral technique is nearly optimal: the computational effort required to solve a diffusion equation for one realization of the potential fields scales as $N_s N_x \log N_x$, where N_s is the number of chain contour steps.

The expressions for the derivatives of the energy functionals are linearly related to density operators, which are, in turn, nonlinearly and nonlocally related to the propagators q and q^\dagger by expressions such as (2.5). These expressions are most conveniently evaluated in real space at the collocation points of the basis functions. Because $q(\mathbf{r}, s; [\mu])$ is evaluated by (3.1) at equally spaced contour positions, a Newton–Cotes formula with comparable accuracy is most convenient for evaluating the contour integrals in expressions such as (2.5). In particular, a composite Simpson’s rule with truncation error that is $O(\Delta s^4)$ is our method of choice. The computational effort to evaluate expressions such as (2.5), (2.9)–(2.10), and (2.19)–(2.20) by such a procedure is evidently comparable to a solution of the diffusion equation, i.e., $O(N_s N_x \log N_x)$.

The problem of converging the chemical potential fields to a minimum or saddle point can be viewed alternatively as a *nonlinear set of equations* to be solved for the spectral elements or collocated fields (e.g., (2.4), (2.11)–(2.12), or (2.23)–(2.24)) or as a *nonlinear optimization problem*. Adopting the first perspective, quasi-Newton methods are often employed when implementing the fully spectral approach to SCFT devised by Matsen and Schick [20]. These techniques, however, scale at best as $O(N_x^3)$. For high-resolution simulations with $N_x \sim 10^3 - 10^6$ spatial modes, such methods are prohibitively expensive. We shall take the perspective in the present paper that any potential field update scheme costing more than $O(N_x \log N_x)$ operations per iteration is unacceptable for large scale computation. The specific approaches to be followed are somewhat model dependent, so we consider them in the subsequent sections on a case-by-case basis.

3.1. Target homopolymer density problem. This problem is the easiest, because $G[\mu]$ has a minimum that corresponds to our desired solution $\mu^*(\mathbf{r})$, and that solution is unique up to a uniform shift. A natural approach is to try a relaxation (iterative) scheme in which we introduce a fictitious “time” variable t and relax down the gradient of G :

$$(3.2) \quad \frac{\partial}{\partial t} \mu(\mathbf{r}, t) = - \frac{\delta G[\mu]}{\delta \mu(\mathbf{r}, t)} = \tilde{\rho}(\mathbf{r}; [\mu(t)]) - \rho(\mathbf{r}).$$

This can be viewed either as a relaxation scheme for solving (2.4) or a continuous steepest descent approach to the problem of minimizing $G[\mu]$. Regardless of the perspective, we should point out that the “dynamics” described by (3.2) are not physical polymer dynamics and that the goal is simply to find the steady state solution $\mu^*(\mathbf{r})$ as quickly and efficiently as possible. Every evaluation of the RHS of this equation involves a solution of the diffusion equation for a fixed value of $\mu(\mathbf{r}, t)$ and subsequent evaluation of the density operator, each costing of order $N_s N_x \log N_x$ operations. Thus, it pays to favor *stability* over accuracy in time integration schemes,

since that allows larger time steps Δt and presumably fewer total iterations (throughout this work the words iteration and relaxation are used interchangeably) to reach the steady state. As a result, a high-order time integration scheme for (3.2), such as a fourth-order Runge–Kutta or a multistep method, would not be appropriate for high-resolution SCFT calculations.

Another issue, noted previously, is that the density operators prove to be invariant to *uniform* shifts in the chemical potential fields. In the case of (3.2) this implies that the $k = 0$ Fourier component of $\mu(\mathbf{r})$ does not relax. Numerical errors can thus accumulate and cause the spatial average of $\mu(\mathbf{r})$ to drift and ultimately create an overflow or underflow situation. This is easily rectified, however, by imposing at each iteration uniform shifts in the potential to pin its mean value at zero. Interestingly, this problem disappears if the polymer theory is reformulated in the grand canonical ensemble.

A very simple and useful *explicit* time integration scheme is the forward Euler formula applied at the half step

$$(3.3) \quad \mu^{j+1/2}(\mathbf{r}) = \mu^j(\mathbf{r}) - \Delta t \frac{\delta G[\mu^j]}{\delta \mu^j(\mathbf{r})},$$

followed by a uniform field shift as described above:

$$(3.4) \quad \mu^{j+1}(\mathbf{r}) = \mu^{j+1/2}(\mathbf{r}) - \frac{1}{V} \int d\mathbf{r} \mu^{j+1/2}(\mathbf{r}).$$

This simple scheme is much more stable than other low-order explicit time stepping algorithms and is quite efficient for target density patterns without large gradients. The integral in the shift (3.4) can be computed with spectral accuracy by simply using the composite trapezoidal rule, as the integrand is periodic.

More stable time stepping algorithms can be constructed by using fully implicit discretizations, i.e., by applying an approximation to $\tilde{\rho}$ at the future, $j + 1/2$, rather than the present time j . Unfortunately such discretizations would yield at each iteration step a nonlinear system of equations for $\mu^{j+1/2}$ whose solution would be as expensive as solving the original equation (2.4). A more efficient approach is to use a semi-implicit discretization in which the leading-order term (at high frequencies) is treated implicitly, while the rest of the RHS is evaluated explicitly. A carefully designed semi-implicit method can allow large step sizes and still retain computational efficiency per step. However, due to the highly nonlocal and nonlinear nature of SCFT equations, such semi-implicit schemes are nontrivial to identify. To obtain a class of these schemes we follow an idea motivated by the small scale decomposition introduced by Hou, Lowengrub, and Shelley [17] in the context of boundary integral methods for interfacial dynamics. A similar idea but for local terms has been used by Badalassi, Cenicer, and Banerjee [1] in phase field methods. We begin by expanding the density operator for rapidly varying potentials, i.e., $\mu(\mathbf{r}/\epsilon)$ for $\epsilon \rightarrow 0$. This is equivalent to an asymptotic expansion for small μ (the so-called random phase approximation expansion [18, 3]). By expanding the solution of (2.3) to first order in μ and substituting into (2.5), it is straightforward to show that

$$(3.5) \quad \tilde{\rho}(\mathbf{r}; [\mu]) = \rho_0 [1 - \int d\mathbf{r}' g(\mathbf{r} - \mathbf{r}') \mu(\mathbf{r}') + O(\mu^2)].$$

The kernel $g(\mathbf{r})$ in this expression decays on the scale of R_g (note that this was the length scale used for nondimensionalization) and is most conveniently expressed in

terms of its Fourier transform

$$(3.6) \quad \hat{g}(k) \equiv \int d\mathbf{r} \exp(i\mathbf{k} \cdot \mathbf{r}) g(\mathbf{r}) = 2(e^{-k^2} + k^2 - 1)/k^4,$$

which is the familiar Debye function [3]. Hence, the Jacobian

$$(3.7) \quad \frac{\delta^2 G[\mu]}{\delta \mu(\mathbf{r}) \delta \mu(\mathbf{r}')} = \rho_0 g(\mathbf{r} - \mathbf{r}') + O(\mu)$$

is diagonal in k -space at large k (small ϵ) and positive definite. Morse [22] has recently used this fact to speed up the computation of the Jacobian required in quasi-Newton schemes for implementing the fully spectral version of SCFT.

With the following shorthand for a convolution, $g * \mu \equiv \int d\mathbf{r}' g(\mathbf{r} - \mathbf{r}') \mu(\mathbf{r}')$, our *semi-implicit* time stepping algorithm can be written as

$$(3.8) \quad \frac{\mu^{j+1/2} - \mu^j}{\Delta t} = -\rho_0 g * \mu^{j+1/2} + \tilde{\rho}([\mu^j]) - \rho + \rho_0 g * \mu^j,$$

followed by the uniform shift of (3.4). Equation (3.8) can be efficiently solved for $\mu^{j+1/2}(\mathbf{r})$ by applying a single FFT-inverse FFT pair, requiring $O(N_x \log N_x)$ operations. The shift of (3.4) can be done directly in Fourier space by setting to zero the zeroth mode of $\mu^{j+1/2}(\mathbf{r})$ before applying the inverse FFT. That is,

$$(3.9) \quad \hat{\mu}^{j+1}(k) = \hat{\mu}^j(k) + \frac{\Delta t}{1 + \Delta t \rho_0 \hat{g}(k)} (\widehat{\tilde{\rho}[\mu^j]} - \rho)(k), \quad k \neq 0,$$

$$(3.10) \quad \hat{\mu}^{j+1}(0) = 0,$$

where the caret denotes Fourier transform. Note that in Fourier space the semi-implicit scheme has the same form as the explicit method but with a frequency-dependent step size $\tau(k) = \Delta t / (1 + \Delta t \rho_0 \hat{g}(k))$ that can be precomputed once. With these considerations the cost of the semi-implicit method is nearly identical to that of the explicit method, as we will see in the numerical experiments. Moreover, for large Δt the step size $\tau(k)$ approaches asymptotically $g(k)^{-1}$ which as (3.7) shows is an approximation to the inverse of the Jacobian at small scales. Thus the semi-implicit relaxation for large Δt can be viewed as a quasi-Newton method at small scales.

A third strategy for obtaining the optimum potential field $\mu^*(\mathbf{r})$ of the target homopolymer density problem is to depart from (3.2) and instead adopt the conjugate gradient method for nonlinear optimization [23]. For the present model, gradients are evaluated as $\rho(\mathbf{r}) - \tilde{\rho}(\mathbf{r}; [\mu])$, and full line minimizations are performed with the functional $G[\mu]$ at each iteration to determine the step length along the search direction. Line minimizations are expensive, with each function evaluation costing $O(N_s N_x \log N_x)$, so it remains to be seen whether this extra computational burden is rewarded by proportionally faster convergence than the other two algorithms. We have implemented both Fletcher–Reeves and Polak–Ribière variants for computing conjugate gradient directions. The Polak–Ribière scheme seems to perform better when the residuals are small, but in general there is little apparent difference in the performance of the two variants. Here we report results using the Polak–Ribière scheme.

3.2. Binary blend model. The relaxation methods described in the previous section can be easily extended to the binary blend model, except that care must be taken to respect the saddle point nature of the SCFT solutions. Specifically, since the free energy functional $F[\mu_+, \mu_-]$ is to be maximized with respect to μ_+ and minimized with respect to μ_- , (3.2) should be generalized to

$$(3.11) \quad \frac{\partial}{\partial t} \mu_+(\mathbf{r}, t) = \frac{\delta F[\mu_+, \mu_-]}{\delta \mu_+(\mathbf{r}, t)},$$

$$(3.12) \quad \frac{\partial}{\partial t} \mu_-(\mathbf{r}, t) = -\frac{\delta F[\mu_+, \mu_-]}{\delta \mu_-(\mathbf{r}, t)},$$

which generates potential field updates up the gradient in the μ_+ coordinate and down the gradient in μ_- . The *explicit* forward Euler scheme is evidently

$$(3.13) \quad \mu_+^{j+1/2}(\mathbf{r}) = \mu_+^j(\mathbf{r}) + \Delta t \frac{\delta F[\mu_+^j, \mu_-^j]}{\delta \mu_+^j(\mathbf{r})},$$

$$(3.14) \quad \mu_-^{j+1/2}(\mathbf{r}) = \mu_-^j(\mathbf{r}) - \Delta t \frac{\delta F[\mu_+^j, \mu_-^j]}{\delta \mu_-^j(\mathbf{r})},$$

where (2.7)–(2.8) are used to evaluate the derivatives. Subsequent shifts analogous to (3.4) are then applied to pin the $k = 0$ components of the two fields to the origin:

$$(3.15) \quad \mu_{\pm}^{j+1}(\mathbf{r}) = \mu_{\pm}^{j+1/2}(\mathbf{r}) - \frac{1}{V} \int d\mathbf{r} \mu_{\pm}^{j+1/2}(\mathbf{r}).$$

Construction of a suitable semi-implicit scheme proves to be slightly more involved. Expanding the functional derivatives to first order in μ_{\pm} leads to

$$(3.16) \quad \frac{\delta F[\mu_+, \mu_-]}{\delta \mu_+(\mathbf{r})} = -g * [\mu_+ + (1 - 2f)\mu_-] + O(\mu_{\pm}^2),$$

$$(3.17) \quad \frac{\delta F[\mu_+, \mu_-]}{\delta \mu_-(\mathbf{r})} = \frac{2}{\chi N} \mu_- - g * [(1 - 2f)\mu_+ + \mu_-] + O(\mu_{\pm}^2).$$

Clearly, the use of (3.16) added and subtracted to the RHS of (3.11) at future and present times, respectively, is stabilizing. However, similar addition and subtraction of (3.17) to the RHS of (3.12) is destabilizing. It is therefore not advantageous to utilize the full linearized form of $\delta F/\delta \mu_-$ at the future time. Also the pressure-like potential μ_+ is the stiffest (least smooth) of the two chemical potentials, and thus it makes sense to relax it first and use its updated value immediately after in the relaxation of μ_- , in the manner of Gauss–Siedel. The following semi-implicit–Siedel (SIS) scheme addresses these issues and offers excellent performance:

$$(3.18) \quad \frac{\mu_+^{j+1/2} - \mu_+^j}{\Delta t} = -g * \mu_+^{j+1/2} + \frac{\delta F[\mu_+^j, \mu_-^j]}{\delta \mu_+^j} + g * \mu_+^j,$$

$$(3.19) \quad \frac{\mu_-^{j+1/2} - \mu_-^j}{\Delta t} = -(2/\chi N) \mu_-^{j+1/2} - \frac{\delta F[\mu_+^{j+1/2}, \mu_-^j]}{\delta \mu_-^j} + (2/\chi N) \mu_-^j,$$

followed by the shifts of (3.15). Equation (3.18) is efficiently solved just as in the target density model by applying an FFT-inverse FFT pair, while (3.19) is trivially implicit, requiring only algebraic manipulations to solve for $\mu_-^{j+1/2}$ on the collocation points in real space. We note that a second solution of the diffusion equations and derivative evaluation is required between (3.18) and (3.19) in order to evaluate $\delta F[\mu_+^{j+1/2}, \mu_-^j]/\delta \mu_-^j$ at the intermediate state of new μ_+ and old μ_- . While this approximately doubles the computational cost per time step over the explicit scheme, we shall see that this semi-implicit algorithm more than compensates by yielding in general a much faster convergence.

Finally, we consider whether an optimization scheme could be applied in place of (3.11) and (3.12) to analyze the blend model. The saddle point nature of the problem prohibits direct application of the conjugate gradient method. A standard approach [23] is to construct an auxiliary functional

$$(3.20) \quad \tilde{F}[\mu_+, \mu_-] = \frac{1}{2} \int d\mathbf{r} \left[\left(\frac{\delta F}{\delta \mu_+(\mathbf{r})} \right)^2 + \left(\frac{\delta F}{\delta \mu_-(\mathbf{r})} \right)^2 \right]$$

that evidently has local minima at solutions of the SCFT equations. Use of this functional, however, has two drawbacks. The first derivatives of \tilde{F} involve the second derivatives of F , which are expensive to compute with $O(N_s N_x^2)$ effort. Moreover, even if one were to approximate the second derivatives of F or attempt to compute them numerically, it appears that the functional \tilde{F} confers an unphysical local stability to the trivial homogeneous solution $\mu_+^* = \mu_-^* = 0$. With analytical approximations to the second derivatives, we found it difficult to converge solutions other than the trivial solution. Since nonlinear optimization of saddle point problems is currently a very active area of research, it may be the case that new methods will become available to apply to saddle point SCFT problems. In the meantime, we expect that efficient time stepping algorithms such as those outlined in this work for the solution of (3.11)–(3.12) will prove to be the methods of choice for analyzing the macrophase separation of homopolymers [3].

3.3. Diblock copolymer model. The development of explicit and semi-implicit time stepping algorithms for the diblock copolymer model closely follows that for the binary blend. Equations (3.11)–(3.12) still apply but with derivatives $\delta F[\mu_\pm]/\delta \mu_\pm$ replaced by $\delta H[\mu_\pm]/\delta \mu_\pm$ given in (2.17)–(2.18). The *explicit* forward Euler scheme is identical to (3.13)–(3.14):

$$(3.21) \quad \mu_+^{j+1/2}(\mathbf{r}) = \mu_+^j(\mathbf{r}) + \Delta t \frac{\delta H[\mu_+^j, \mu_-^j]}{\delta \mu_+^j(\mathbf{r})},$$

$$(3.22) \quad \mu_-^{j+1/2}(\mathbf{r}) = \mu_-^j(\mathbf{r}) - \Delta t \frac{\delta H[\mu_+^j, \mu_-^j]}{\delta \mu_-^j(\mathbf{r})},$$

followed by the shifts of (3.15).

To develop a semi-implicit scheme, it is again helpful to expand the derivatives to first order in μ_\pm . We find that

$$(3.23) \quad \frac{\delta H[\mu_+, \mu_-]}{\delta \mu_+(\mathbf{r})} = -(g_{AA} + 2g_{AB} + g_{BB}) * \mu_+ + (g_{AA} - g_{BB}) * \mu_- + O(\mu_\pm^2),$$

$$(3.24) \quad \frac{\delta H[\mu_+, \mu_-]}{\delta \mu_-(\mathbf{r})} = \frac{2}{\chi N} \mu_- + (g_{AA} - g_{BB}) * \mu_+ - (g_{AA} - 2g_{AB} + g_{BB}) * \mu_- + O(\mu_\pm^2),$$

where again $*$ denotes convolution and the symmetric 2×2 matrix of kernels is most conveniently expressed as Fourier transforms:

$$(3.25) \quad \hat{g}_{AA}(k) = \frac{2}{k^4} [fk^2 + \exp(-k^2 f) - 1],$$

$$(3.26) \quad \hat{g}_{AB}(k) = \frac{1}{k^4} [1 - \exp(-k^2 f)][1 - \exp(-k^2(1 - f))],$$

$$(3.27) \quad \hat{g}_{BB}(k) = \frac{2}{k^4} [(1 - f)k^2 + \exp(-k^2(1 - f)) - 1].$$

These functions are well known as the relevant Debye scattering functions for diblock copolymers [18]. Following the same arguments as those used to deduce the blend algorithm described in (3.18)–(3.19), we propose the following SIS scheme for the diblock melt:

$$(3.28) \quad \frac{\mu_+^{j+1/2} - \mu_+^j}{\Delta t} = -(g_{AA} + 2g_{AB} + g_{BB}) * \mu_+^{j+1/2} + \frac{\delta H[\mu_+^j, \mu_-^j]}{\delta \mu_+^j} \\ + (g_{AA} + 2g_{AB} + g_{BB}) * \mu_+^j,$$

$$(3.29) \quad \frac{\mu_-^{j+1/2} - \mu_-^j}{\Delta t} = -(2/\chi N)\mu_-^{j+1/2} - \frac{\delta H[\mu_+^{j+1/2}, \mu_-^j]}{\delta \mu_-^j} + (2/\chi N)\mu_-^j,$$

followed by the zeroth mode shifts. As in the blend case, a second solution of the diffusion equations (2.15) and (2.21) and density operator evaluation according to (2.19)–(2.20) is required before applying (3.29) in order to evaluate $\delta H[\mu_+^{j+1/2}, \mu_-^j]/\delta \mu_-^j$ for the updated pressure field $\mu_+^{j+1/2}$. Equations (3.28) and (3.29) have the same structure as in the SIS method for the blend, and thus they can be solved efficiently in exactly the same way for analyzing the microphase separation of block copolymers [3].

3.4. Multilevel embedding. One can view (2.4) for the optimal field $\mu^*(\mathbf{r})$ as a nonlinear equation, and, as such, one is naturally tempted to try the nonlinear multigrid algorithm [2]. The efficacy of nonlinear multigrid relies heavily on having a relaxation method that quickly damps high-frequency components of the error. However, due to the highly nonlocal nature of (2.4) (and of the SCFT equations in general) such relaxation methods would be extremely difficult and computationally expensive to achieve. The semi-implicit small scale decomposition that we propose here does a stronger high-modal damping in the error than the explicit Euler technique, but both schemes primarily enhance the damping of low-frequency modes. The conjugate gradient method is itself a roughening algorithm. Thus, the fine-to-coarse grid process of the multigrid method for the purpose of a coarse grid correction of the error would not work in the present context of the SCFT equations. However, one can still use coarse grid information to construct an initial guess for the fine grid iteration, i.e., a coarse-to-fine process. Moreover, we can apply this strategy in a multilevel fashion and to all the iterative relaxation schemes for solving the SCFT equations.

To simplify the description of our multilevel approach let us consider the simplest case of finding the chemical potential field for a prescribed inhomogeneous density, i.e., the problem of section 2.1. Let us assume a uniform discretization and denote by N_x and N_s the number of spatial nodes (collocation points) and the number of chain contour steps, respectively. (N_x, N_s) defines the finest grid level, and, assuming that

N_x and N_s are powers of two, one can choose the coarsest level (N_x^0, N_s^0) such that $(N_x, N_s) = (2^L N_x^0, 2^L N_s^0)$, where L is an integer. This will give us $L + 1$ grid levels:

$$(3.30) \quad (N_x^l, N_s^l) = (2^l N_x^0, 2^l N_s^0), \quad l = 0, 1, \dots, L,$$

with $(N_x^L, N_s^L) = (N_x, N_s)$.

Since the unconditionally stable scheme (3.1) is used, we are only constrained by accuracy and efficiency in choosing N_s^l . Given the high-order accuracy of our discretization these two requirements can be accomplished by taking $N_s^l \propto N_x^l$. Thus, we can label each grid level with just one of these two parameters. Let $\mu_{N_x^l}^{(0)}$ be the initial guess of the chemical potential at a given resolution N_x^l , and denote by $R_{m_l}[\mu_{N_x^l}^{(0)}]$ the result of applying m_l (explicit or semi-implicit) relaxations ("time" steps) to it. With this notation the multilevel embedding algorithm can be described simply as follows:

1. Input initial guess at coarsest level, $\mu_{N_x^0}^{(0)}$.
2. For $l = 0 : L - 1$, relax and interpolate to next finer level:

$$(3.31) \quad \mu_{N_x^l}^{(1)} = R_{m_l}[\mu_{N_x^l}^{(0)}];$$

$$(3.32) \quad \mu_{N_x^{l+1}}^{(0)} = I_{N_x^l}^{2N_x^l}[\mu_{N_x^l}^{(1)}];$$

3. Starting with $\mu_{N_x^L}^{(0)}$, relax at finest level until the desired tolerance in the error is met.

In (3.32), $I_{N_x^l}^{2N_x^l}$ stands for spatial interpolation from grid level l to grid level $l + 1$. Spectral interpolation in this case can be efficiently implemented by just padding with zeros the Fourier transform of $\mu_{N_x^l}^{(1)}$ to correspond to that of a $2N_x^l$ long array and transforming back.

The number of relaxations per level m_l should be chosen such that at the end only a few finest grid relaxations are needed to achieve a given tolerance. Thus, for computational efficiency m_l should decrease with l . Here we choose

$$(3.33) \quad m_l = \frac{M}{2^l}, \quad l = 0, 1, \dots, L - 1,$$

where M is the number of relaxations at the coarsest level. Clearly, the choice of M depends on the problem, the particular relaxation scheme used, and the desired tolerance. An appropriate M can be predetermined by running fast coarse grid relaxations. Here we illustrate only the potential of this technique without fine-tuning the number of sweeps m_l .

4. Results. We now examine the performance of the above schemes with a series of numerical experiments in one spatial dimension for each model. All the methods considered here have been implemented in FORTRAN. Fourier transforms are computed using the FFTW [12] package. The codes were run in the same dedicated computer, a Pentium III 1GHz 2Gb RAM workstation under linux. The step size, Δt , is always selected as large as the stability of the methods permits and so that the error is decreased the fastest.

4.1. Target homopolymer density problem. For this model we consider the following target density:

$$(4.1) \quad \rho(r) = \rho_0[1 + \tanh(\eta \cos(2\pi L^{-1}r))], \quad 0 \leq r \leq L,$$

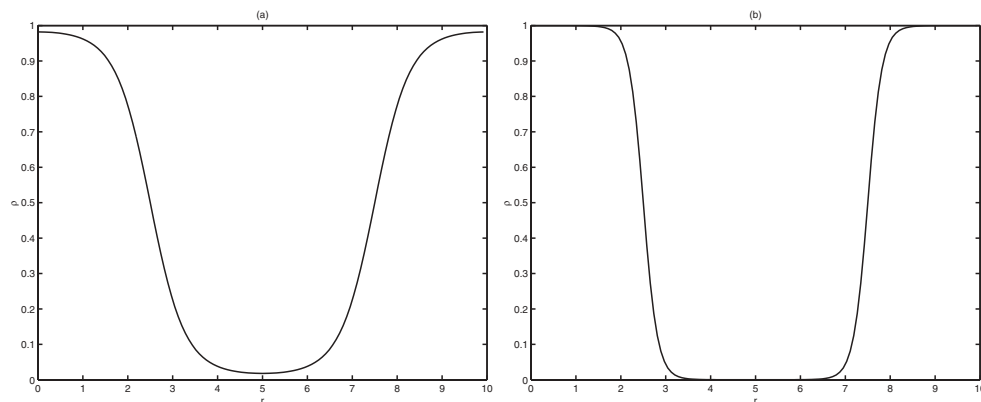


FIG. 1. Target homopolymer density $\rho(r)$. (a) $\eta = 2$ and (b) $\eta = 5$.

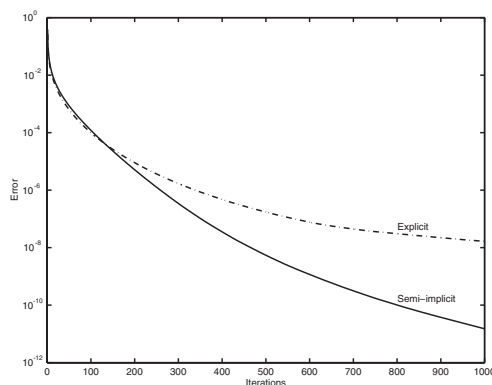


FIG. 2. Target homopolymer density model; $\eta = 2$. Error for explicit (dashed-dotted curve) and semi-implicit (continuous curve) methods.

where ρ_0 is the volume-averaged monomer density, η is a constant, and L is the domain size. We take $L = 10$ and $\rho_0 = 1/2$ and consider two values of η , 2 and 5, which correspond to a smooth target and a “sharper” target, respectively, as shown in Figure 1. We set initially $\mu(r) \equiv 0$. To measure the error we use the l_1 norm

$$(4.2) \quad |f|_1 \equiv \frac{1}{N_x} \sum_{j=1}^{N_x} |f(r_j)|.$$

Figure 2 shows the error $|\rho - \tilde{\rho}|_1$ in the case of $\eta = 2$ against the number of iterations for both the explicit Euler relaxation and the semi-implicit scheme with $\Delta t = 2.5$ and $\Delta t = 21$, respectively. $N_x = 128$ and $N_s = N_x$ are used for both schemes. Because in Fourier space the semi-implicit scheme becomes explicit, its computational cost is nearly the same as that of the explicit method. Indeed, 1000 iterations took 2.040sec for the explicit and 2.050sec for the semi-implicit. As observed in Figure 2 the schemes are comparable up to errors of $O(10^{-4})$ where a crossover takes place and the faster decay of the semi-implicit outperforms the explicit relaxation. Table 1 compares the explicit, semi-implicit, and conjugate gradient methods. The conjugate gradient method has the fastest rate of convergence, but, because it requires

TABLE 1

Target homopolymer density model; $\eta = 2$. Comparison of the one-level schemes. NC denotes no convergence to a particular error level.

Error	Explicit		Semi-implicit		Conjugate gradient	
	Iterations	CPU time(sec)	Iterations	CPU time(sec)	Iterations	CPU time(sec)
10^{-3}	41	0.10	47	0.11	11	0.22
10^{-5}	195	0.41	175	0.37	32	0.56
10^{-8}	1194	2.43	452	0.93	NC	—
10^{-12}	7721	15.74	1274	2.57	NC	—

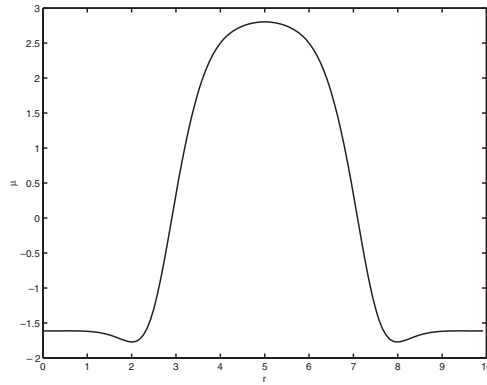
FIG. 3. Solution μ for the target homopolymer density model; $\eta = 2$.

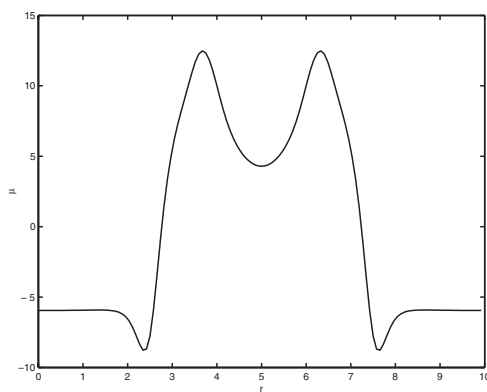
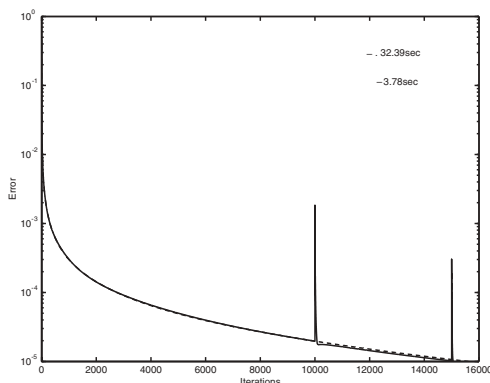
TABLE 2

Target homopolymer density model; $\eta = 5$. Comparison of the one-level schemes.

Error	Explicit		Semi-implicit		Conjugate gradient	
	Iterations	CPU time(sec)	Iterations	CPU time(sec)	Iterations	CPU time(sec)
10^{-3}	313	0.69	307	0.65	48	0.87
10^{-4}	2743	5.56	2753	5.62	145	2.48
10^{-5}	14854	29.38	15607	32.39	4875	8.67

an average of 10 to 11 energy function evaluations for the line minimization per iteration, it performs the poorest for this particular case. Moreover, the conjugate gradient method stalls at an error level of 10^{-7} . Note that for an error less than 10^{-12} the semi-implicit scheme converges 6 times faster than the explicit one. The numerical solution μ with $|\rho - \tilde{\rho}|_1 = 10^{-12}$ is shown in Figure 3.

We now turn to $\eta = 5$. As Table 2 shows, for this sharper target, the explicit method ($\Delta t = 2.5$) and the semi-implicit scheme ($\Delta t = 19$) have a comparable performance with a much slower convergence rate than that observed for $\eta = 2$. Note also that at high accuracy the conjugate gradient method performs the best of the three methods, reaching an error of 10^{-5} almost 4 times faster than the other two schemes. The numerical solution μ with $|\rho - \tilde{\rho}|_1 = 10^{-5}$ is shown in Figure 4. This is a much less smooth function than that for $\eta = 2$ and thus with more high-modal components, which explains the slowdown in the convergence of the two descent-type methods. As a consequence of the slow convergence rate, the computational cost for finding μ in the case of a sharp target density can put a serious constraint on high-resolution

FIG. 4. Solution μ for the target homopolymer density model; $\eta = 5$.FIG. 5. Target homopolymer density model; $\eta = 5$. Comparison of the one-level semi-implicit scheme (dashed-dotted curve) and its multi-level version (continuous curve).

computations, especially in multidimensions. We can cut down significantly the computational cost by using the multilevel strategy described in section 3.4. Figure 5 shows the behavior of the error for the semi-implicit scheme (dashed-dotted curve) and for its multilevel (continuous curve) version. The coarsest grid is $N_x^0 = 32$, and thus three levels are used in this case. There are jumps in the error when a change of level is performed and interpolation is employed, but the error quickly goes back to its one-level decaying rate that is approximately independent of the resolution (N_x, N_s). The multilevel algorithm takes 3.74sec to achieve an accuracy of 10^{-5} in the error, almost one ninth of the time employed by the one-level scheme.

4.2. Binary blend model. We start with $\chi N = 4$, $L = 10$, and the symmetric case $f = 1/2$. We first use the following initial conditions for the chemical potentials:

$$(4.3) \quad \mu_-(r) = 0.1 \cos(2\pi L^{-1}r),$$

$$(4.4) \quad \mu_+(r) = -0.1 \cos(2\pi L^{-1}r).$$

We fix the (finest) resolution to $N_x = 256$ and $N_s = N_x$. Figure 6 demonstrates the superiority of the SIS scheme ($\Delta t = 50$) over the explicit relaxation ($\Delta t = 1.5$). Even though the SIS costs roughly twice as much as the explicit scheme per iteration,

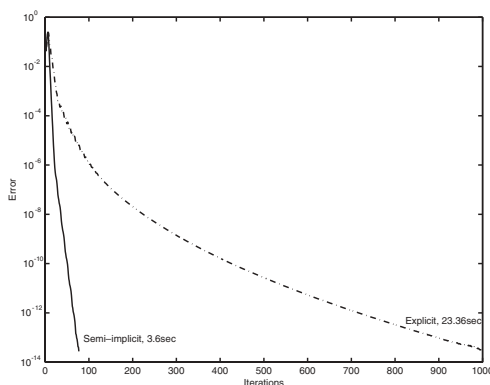


FIG. 6. Binary blend model; $\chi N = 4$, $f = 1/2$, $L = 10$. Deterministic initial conditions. Comparison of the SIS scheme (continuous curve) and the explicit Euler scheme (dashed-dotted curve).

TABLE 3

Binary blend model; $\chi N = 4$, $f = 1/2$, $L = 10$, $N_x = 256$, and $N_s = N_x$. In the ML-SIS, A/B , A is the number of finest grid iterations and B is the total number of iterations.

Error	Explicit		SIS		ML-SIS	
	Iterations	CPU time(sec)	Iterations	CPU time(sec)	Iterations	CPU time(sec)
10^{-3}	26	0.61	14	0.65	1/15	0.10
10^{-5}	70	1.55	19	0.89	2/30	0.18
10^{-8}	225	5.27	36	1.68	10/76	0.60
10^{-12}	717	16.50	65	2.94	21/143	1.21

its fast convergence quickly compensates the extra work converging to $O(10^{-14})$ almost 6.5 times faster. Table 3 presents a comparison of these two methods along with the multilevel SIS. Again for the latter, $N_x^0 = 32$ was used, and thus the computations were performed using four levels. The multilevel embedding of the SIS method can further speed up the computations by reducing the number of finest grid iterations. As Table 3 shows, the multilevel SIS (ML-SIS) can be over 13 times faster than the explicit method at an error of 10^{-12} . The local monomer volume fractions and the approximations to the saddle point fields μ_-^* and μ_+^* are shown in Figure 7. As anticipated in constructing the SIS scheme, μ_-^* is smoother than μ_+^* , which has pronounced cusps in the interfacial regions.

The performance difference between the explicit and the SIS methods is even greater in the case of random initial conditions for the chemical potentials, as illustrated in Figure 8. It takes the explicit scheme 1000 iterations (22.67sec) to reduce the error to $O(10^{-6})$, while the SIS method accomplishes this in 40 iterations (1.82sec), i.e., over 12 times faster. With the random initial conditions for the chemical potentials, a different solution is selected as shown in Figure 9. The same pattern is selected by the explicit, the SIS, and the ML-SIS method. The ML-SIS converges to this solution, in a fraction of the SIS time.

We now consider larger χN , i.e., stronger segregation of the A and B polymer segments, and larger domain size L . We take $\chi N = 8$, $L = 20$, and $f = 1/2$ with initial conditions (4.3) and (4.4). Figure 10 presents the error plotted against the number of iterations. The error for the explicit method ($\Delta t = 0.25$) shows an oscillatory

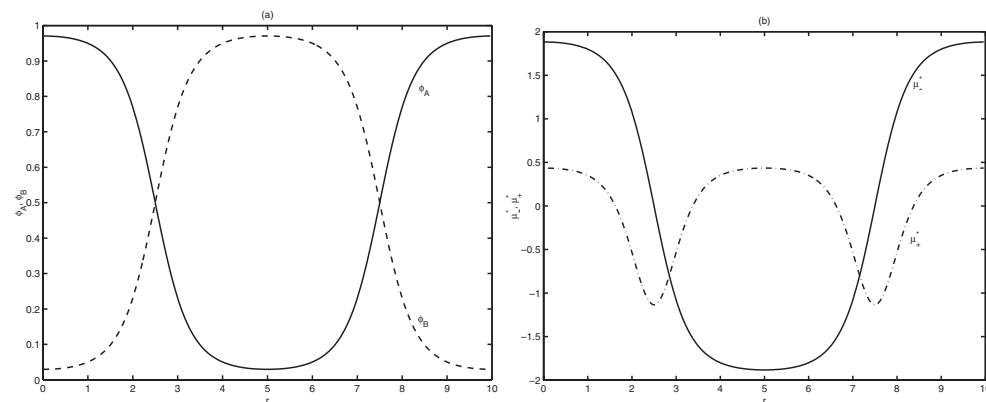


FIG. 7. Binary blend model; $\chi N = 4$, $f = 1/2$, $L = 10$. Deterministic initial conditions. (a) $\tilde{\phi}_A$ and $\tilde{\phi}_B$. (b) μ_-^* and μ_+^* . Error = 10^{-12} .

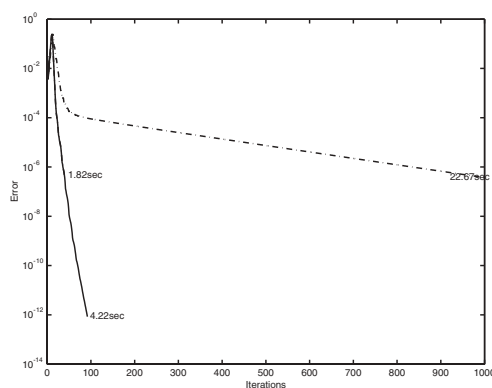


FIG. 8. Binary blend model; $\chi N = 4$, $f = 1/2$, $L = 10$. Random initial conditions. Comparison of the SIS scheme (continuous curve) and the explicit Euler scheme (dashed-dotted curve).

behavior, and its minimum value after 500 iterations is only 2.5×10^{-3} . The SIS scheme ($\Delta t = 50$) converges quickly, reaching an error of 2×10^{-13} after 500 iterations in 22.88sec of CPU time. The ML-SIS scheme with $N_x^0 = 64$ (three levels) can reach the same accuracy in just 6.05sec. The numerical solutions are shown in Figure 11. A similar performance of the methods is observed for the asymmetric case. The solution for $f = 0.3$ is presented in Figure 12. The explicit scheme fails to converge below 5×10^{-3} , while the SIS method reaches an error of 4×10^{-13} at the end of the 500 iterations. The superiority of the SIS scheme over the explicit method is again even greater in the case of random initial conditions. The explicit scheme fails to converge below an error of 10^{-2} , while the SIS scheme converges quickly up to round-off error level in 650 iterations with $\Delta t = 25$.

4.3. Diblock copolymer model. We consider first for this model the case $\chi N = 16$, $L = 10$, $f = 1/2$, and random initial conditions for the potentials. We take again the (finest) resolution to be $N_x = 256$ and $N_s = N_x$. Figure 13 compares the behavior of the error for the explicit ($\Delta t = 4$) and the SIS ($\Delta t = 500$) schemes. The detailed performance of the methods is listed in Table 4, where representative

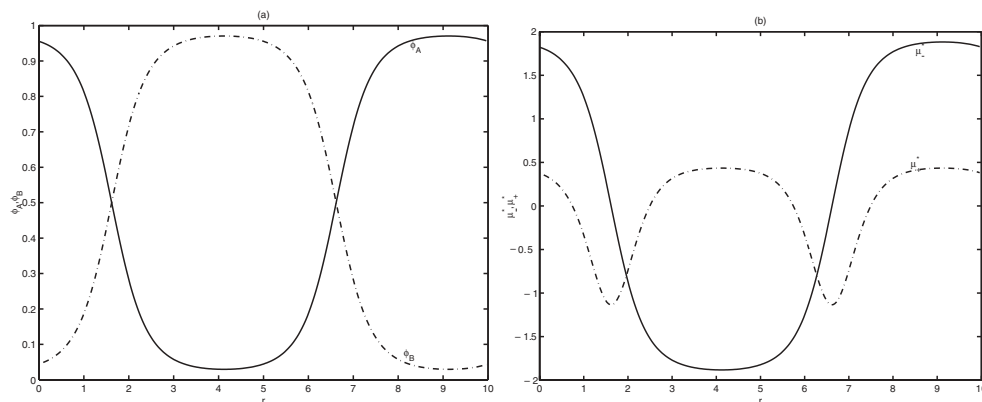


FIG. 9. Binary blend model; $\chi N = 4$, $f = 1/2$, $L = 10$. Random initial conditions. (a) ϕ_A and ϕ_B . (b) μ_-^* and μ_+^* . Error = 1×10^{-14} .

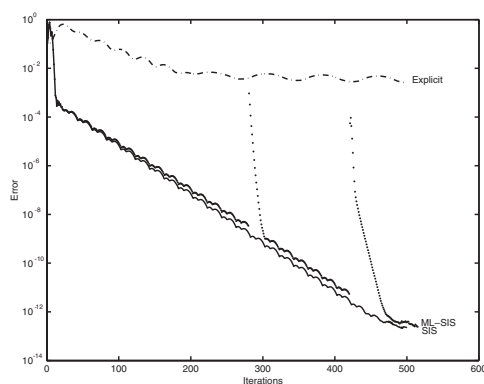


FIG. 10. Binary blend model; $\chi N = 8$, $f = 1/2$, $L = 20$. Deterministic initial conditions. Comparison of the SIS scheme (continuous curve) and the explicit Euler scheme (dashed-dotted curve) and the ML-SIS scheme (dotted).

multilevel numbers are also shown. For this χN the explicit and the SIS schemes are comparable at low accuracy ($O(10^{-5})$). At high accuracy the SIS scheme becomes more than twice as fast as the explicit method. The SIS scheme reaches round-off error level at about 350 iterations. For an error of 10^{-12} the ML-SIS (with four levels) cuts down the computational cost of the one-level SIS by a factor of more than 6 and by over a factor of 12 for the explicit method. Figure 14 shows the solution for an error equal to 10^{-12} .

We now increase the χN parameter and reduce the domain size as follows: $\chi N = 25$, $L = 5$. Again we consider the symmetric case $f = 1/2$ and random initial conditions for the potentials. The error plotted against the number of iterations for the explicit method ($\Delta t = 4$) and for the SIS relaxation ($\Delta t = 500$) appears in Figure 15. The two methods give now a slightly slower error decay, and the explicit scheme presents a different behavior at the first 200 iterations before going to a steady monotone decay. The detailed comparison of their performance at several accuracies is presented in Table 5. At high accuracy, the SIS method is still superior to the explicit relaxation and for an error = 10^{-12} is over twice as fast. The solution

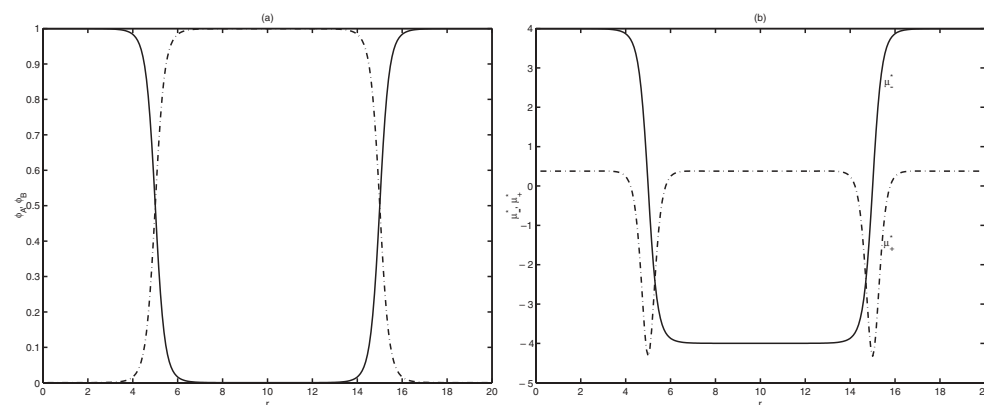


FIG. 11. *Binary blend model*; $\chi N = 8$, $f = 1/2$, $L = 20$. (a) $\tilde{\phi}_A$ and $\tilde{\phi}_B$. (b) μ_-^* and μ_+^* . Error = 2×10^{-13} .

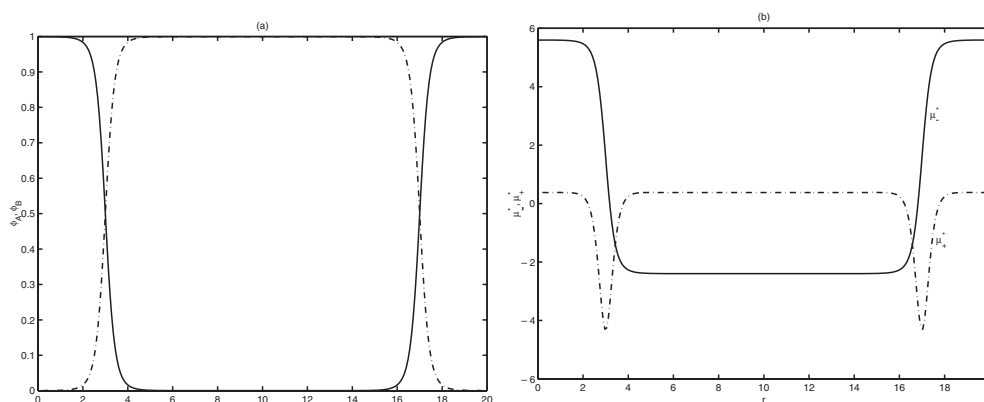


FIG. 12. *Binary blend model*; $\chi N = 8$, $f = 0.3$ (asymmetric), $L = 20$. (a) $\tilde{\phi}_A$ and $\tilde{\phi}_B$. (b) μ_-^* and μ_+^* . Error = 4×10^{-13} .

is shown in Figure 16.

As the last case we consider larger χN . We take $\chi N = 40$, $L = 5$, $f = 1/2$, and random initial conditions. Figure 17 compares the decay rate of the error for the explicit method ($\Delta t = 1$) and for the SIS scheme ($\Delta t = 20$). At this χN , the explicit Euler method fails to converge below an error of $O(10^{-3})$, while the SIS scheme can easily attain an error at round-off level in a few hundred iterations. Figure 18 compares the SIS with its multilevel version for the case of three levels and $\Delta t = 40$. The SIS reaches an error of 10^{-10} in 20.06sec, while the ML-SIS can reach such accuracy in 5.54sec. The solution is shown in Figure 19.

5. Discussion and conclusions. We presented and examined several numerical methods for solving the self-consistent mean-field equations for inhomogeneous polymers in three illustrative problems. A new class of efficient semi-implicit methods and a multilevel strategy were proposed. At high accuracy, the semi-implicit methods consistently outperform the explicit relaxation scheme. When random conditions and/or strongly segregated polymers are considered, the superiority of the semi-implicit schemes is even more pronounced. Furthermore, by embedding the new

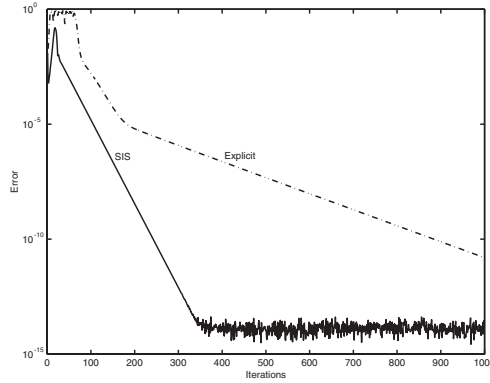


FIG. 13. Copolymer melt model; $\chi N = 16$, $f = 1/2$, $L = 10$. Random initial conditions. Comparison of the SIS scheme (continuous curve) and the explicit Euler scheme (dashed-dotted curve).

TABLE 4

Copolymer blend model; $\chi N = 16$, $f = 1/2$, $L = 10$, $N_x = 256$, and $N_s = N_x$. In the ML-SIS (four levels, $\Delta t = 200$), A/B , A is the number of finest grid iterations and B is the total number of iterations.

Error	Explicit		SIS		ML-SIS	
	Iterations	CPU time(sec)	Iterations	CPU time(sec)	Iterations	CPU time(sec)
10^{-3}	108	2.34	24	1.06	1/43	0.15
10^{-5}	183	4.00	106	4.59	6/110	0.50
10^{-8}	587	12.97	188	8.03	15/190	0.99
10^{-12}	1173	25.43	298	12.77	23/338	1.64

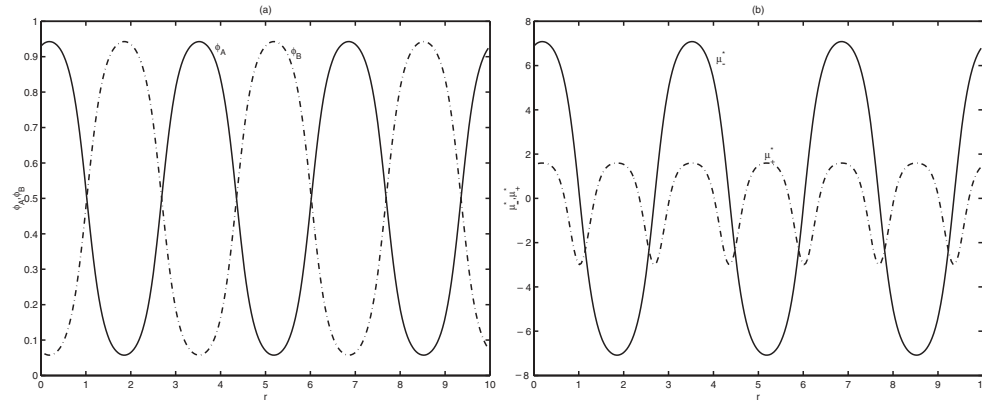


FIG. 14. Copolymer melt model; $\chi N = 16$, $f = 1/2$, $L = 10$. Random initial conditions. (a) $\bar{\phi}_A$ and $\bar{\phi}_B$. (b) μ_-^* and μ_+^* . Error = 1×10^{-12} .

semi-implicit relaxation schemes into the proposed multilevel strategy, we obtained methods that can achieve computational savings of as much as an order of magnitude for the one-dimensional problems studied here. We expect that the multilevel strategy will be even more beneficial when scaling up to high-resolution SCFT simulations in two and three dimensions [27]. Finally, we note that an alternative SCFT relaxation

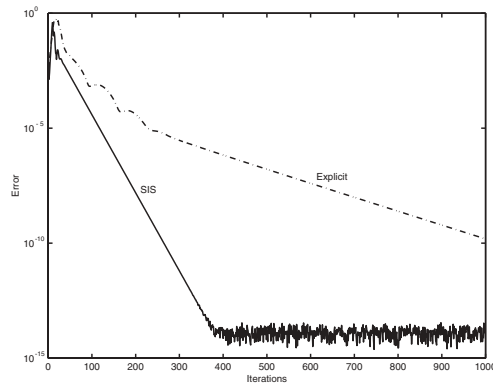


FIG. 15. Copolymer melt model; $\chi N = 25$, $f = 1/2$, $L = 5$. Random initial conditions. Comparison of the SIS scheme (continuous curve) and the explicit Euler scheme (dashed-dotted curve).

TABLE 5

Copolymer blend model; $\chi N = 25$, $f = 1/2$, $L = 5$, $N_x = 256$, and $N_s = N_x$. In the ML-SIS (four levels, $\Delta t = 80$), A/B , A is the number of finest grid iterations and B is the total number of iterations.

Error	Explicit		SIS		ML-SIS	
	Iterations	CPU time(sec)	Iterations	CPU time(sec)	Iterations	CPU time(sec)
10^{-3}	89	1.93	59	2.58	2/72	0.25
10^{-5}	229	4.95	118	5.13	7/136	0.58
10^{-8}	699	15.00	206	9.01	21/231	1.36
10^{-12}	1365	29.62	324	13.92	43/375	2.54

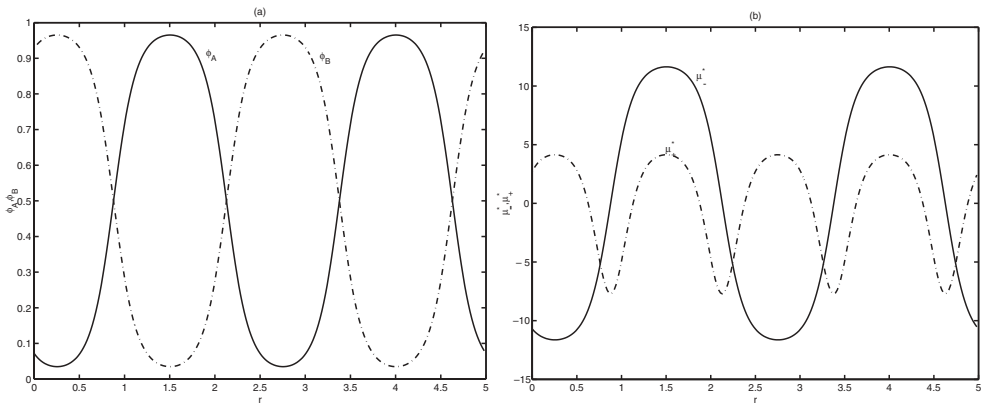


FIG. 16. Copolymer melt model; $\chi N = 25$, $f = 1/2$, $L = 5$. Random initial conditions. (a) $\bar{\phi}_A$ and $\bar{\phi}_B$. (b) μ_-^* and μ_+^* . Error = 1×10^{-12} .

scheme employing Anderson mixing has been proposed by Thompson, Rasmussen, and Lookman [28]. This scheme might be fruitfully combined with the multilevel strategy described here.

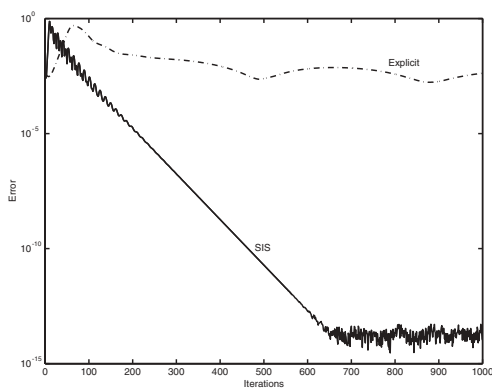


FIG. 17. Copolymer melt model; $\chi N = 40$, $f = 1/2$, $L = 5$. Random initial conditions. Comparison of the SIS scheme (continuous curve) and the explicit Euler scheme (dashed-dotted curve).

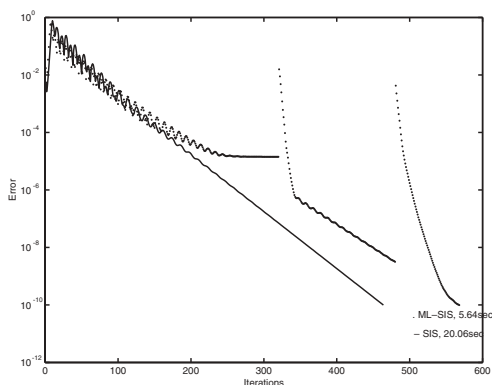


FIG. 18. Copolymer melt model; $\chi N = 40$, $f = 1/2$, $L = 5$. Random initial conditions. The SIS scheme (continuous curve) and the ML-SIS (dotted curve).

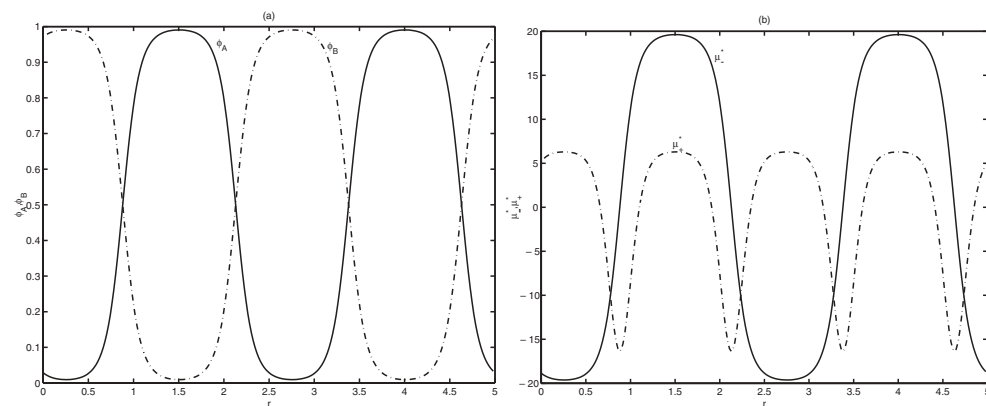


FIG. 19. Copolymer melt model; $\chi N = 40$, $f = 1/2$, $L = 5$. Random initial conditions. (a) $\bar{\phi}_A$ and $\bar{\phi}_B$. (b) μ_-^* and μ_+^* . Error = 1×10^{-12} .

REFERENCES

- [1] V. E. BADALASSI, H. D. CENICEROS, AND S. BANERJEE, *Computation of multiphase systems with phase field models*, J. Comput. Phys., 190 (2003), pp. 371–397.
- [2] A. BRANDT, *Multi-level adaptive solutions to boundary-value problems*, Math. Comp., 31 (1977), pp. 333–390.
- [3] P. G. DE GENNES, *Scaling Concepts in Polymer Physics*, Cornell University Press, Ithaca, NY, 1979.
- [4] M. DOI AND S. F. EDWARDS, *The Theory of Polymer Dynamics*, Oxford University Press, New York, 1986.
- [5] F. DROLET AND G. H. FREDRICKSON, *Combinatorial screening of complex block copolymer assembly with self-consistent field theory*, Phys. Rev. Lett., 83 (1999), pp. 4317–4320.
- [6] F. DROLET AND G. H. FREDRICKSON, *Optimizing chain bridging in complex block copolymers*, Macromolecules, 34 (2001), pp. 5317–5324.
- [7] D. DÜCHS, V. GANESAN, G. H. FREDRICKSON, AND F. SCHMID, *Fluctuation effects in ternary AB+A+B polymeric emulsions*, Macromolecules, 36 (2003), pp. 9237–9248.
- [8] J. FRAAIJE, *Dynamic density functional theory for microphase separation kinetics of block copolymer melts*, J. Chem. Phys., 99 (1993), pp. 9202–9212.
- [9] J. FRAAIJE, B. A. C. VAN VLIEMEREN, N. M. MAURITS, M. POSTMA, O. A. EVERS, C. HOFFMANN, P. ALTEVOGT, AND G. GOLDBECK-WOOD, *The dynamic mean-field density functional method and its application to the mesoscopic dynamics of quenched block copolymer melts*, J. Chem. Phys., 106 (1997), pp. 4260–4269.
- [10] G. H. FREDRICKSON, *Dynamics and rheology of inhomogeneous polymeric fluids: A complex Langevin approach*, J. Chem. Phys., 117 (2002), pp. 6810–6820.
- [11] G. H. FREDRICKSON, V. GANESAN, AND F. DROLET, *Field-theoretic computer simulation methods for polymers and complex fluids [review]*, Macromolecules, 35 (2002), pp. 16–39.
- [12] M. FRIGO AND S. JOHNSON, *FFTW: An adaptive software architecture for the FFT*, ICASSP Conf. Proc., 3 (1998), pp. 1381–1384.
- [13] V. GANESAN AND G. H. FREDRICKSON, *Field-theoretic polymer simulations*, Europhys. Lett., 55 (2001), pp. 814–820.
- [14] D. GOTTLIEB AND S. A. ORSZAG, *Numerical Analysis of Spectral Methods: Theory and Applications*, CBMS-NSF Regional Conf. Ser. Appl. Math. 26, SIAM, Philadelphia, 1977.
- [15] E. HELFAND, *Theory of inhomogeneous polymers: Fundamentals of the Gaussian random-walk model*, J. Chem. Phys., 62 (1975), pp. 999–1005.
- [16] K. M. HONG AND J. NOOLANDI, *Theory of inhomogeneous multicomponent polymer systems*, Macromolecules, 14 (1981), pp. 727–736.
- [17] T. Y. HOU, J. S. LOWENGRUB, AND M. J. SHELLEY, *Removing the stiffness from interfacial flows with surface tension*, J. Comput. Phys., 114 (1994), pp. 312–338.
- [18] L. LEIBLER, *The theory of microphase separation in block copolymers*, Macromolecules, 13 (1980), pp. 1602–1617.
- [19] M. W. MATSEN, *The standard Gaussian model for block copolymer melts*, J. Physics-Condensed Matter, 14 (2002), pp. R21–R47.
- [20] M. W. MATSEN AND M. SCHICK, *Stable and unstable phases of a diblock copolymer melt*, Phys. Rev. Lett., 72 (1994), pp. 2660–2663.
- [21] M. W. MATSEN AND M. SCHICK, *Self-assembly of block copolymers*, Current Opinion in Colloid & Interface Science, 1 (1996), pp. 329–336.
- [22] D. C. MORSE, *private communication*.
- [23] J. NOCEDAL AND S. J. WRIGHT, *Numerical Optimization*, Springer, New York, 1999.
- [24] K. O. RASMUSSEN AND G. KALOSAKAS, *Improved numerical algorithm for exploring block copolymer mesophases*, J. Polymer Science Part B-Polymer Physics, 40 (2002), pp. 1777–1783.
- [25] J. M. H. M. SCHEUTJENS AND G. J. FLEER, *Statistical theory of the adsorption of interacting chain molecules. 1. Partition function, segment density distribution, and adsorption isotherms*, J. Chem. Phys., 83 (1979), pp. 1619–1635.
- [26] A. C. SHI, J. NOOLANDI, AND R. C. DESAI, *Theory of anisotropic fluctuations in ordered block copolymer phases*, Macromolecules, 29 (1996), pp. 6487–6504.
- [27] S. W. SIDES AND G. H. FREDRICKSON, *Parallel algorithm for numerical self-consistent field theory simulations of block copolymer structure*, Polymer, 44 (2003), pp. 5859–5866.
- [28] R. B. THOMPSON, K. O. RASMUSSEN, AND T. LOOKMAN, *Improved convergence in block copolymer self-consistent field theory by Anderson mixing*, J. Chem. Phys., 120 (2004), pp. 31–34.
- [29] M. D. WHITMORE AND J. D. VAVASOUR, *Self-consistent mean field theory of microphases of diblock copolymers*, Macromolecules, 25 (1992), pp. 5477–5486.